NIST Author Manuscript

Continuum of quantum fluctuations in a three-dimensional *S* = 1 Heisenberg magnet

K. W. Plumb[1,2,*], **Hitesh J. Changlani**[2], **A. Scheie**[2], **Shu Zhang**[2], **J. W. Krizan**[3], **J. A. Rodriguez-Rivera**[4,5], **Yiming Qiu**[4], **B. Winn**[6], **R. J. Cava**[3], **C. L. Broholm**[2,4,7]

[1]Department of Physics, Brown University, Providence, RI, USA.

[2]Institute for Quantum Matter and Department of Physics and Astronomy, The Johns Hopkins University, Baltimore, MD, USA.

[3]Department of Chemistry, Princeton University, Princeton, NJ, USA.

[4]NIST Center for Neutron Research, National Institute of Standards and Technology, Gaithersburg, MD, USA.

[5]Department of Materials Science and Engineering, University of Maryland, College Park, MD, USA.

[6]NScD Division, Oak Ridge National Laboratory, Oak Ridge, TN, USA.

[7]Quantum Condensed Matter Division, Oak Ridge National Laboratory, Oak Ridge, TN, USA.

Abstract

Conventional crystalline magnets are characterized by symmetry breaking and normal modes of excitation called magnons, with quantized angular momentum $\hbar$. Neutron scattering correspondingly features extra magnetic Bragg diffraction at low temperatures and dispersive inelastic scattering associated with single magnon creation and annihilation. Exceptions are anticipated in so-called quantum spin liquids, as exemplified by the one-dimensional spin-1/2 chain, which has no magnetic order and where magnons accordingly fractionalize into spinons with angular momentum $\hbar/2$. This is spectacularly revealed by a continuum of inelastic neutron scattering associated with two-spinon processes. Here, we report evidence for these key features of a quantum spin liquid in the three-dimensional antiferromagnet $NaCaNi_2F_7$. We show that despite the complication of random Na^{1+}–Ca^{2+} charge disorder, $NaCaNi_2F_7$ is an almost ideal realization of the spin-1 antiferromagnetic Heisenberg model on a pyrochlore lattice. Magnetic

Bragg diffraction is absent and 90% of the neutron spectral weight forms a continuum of magnetic scattering with low-energy pinch points, indicating $NaCaNi_2F_7$ is in a Coulomb-like phase. Our results demonstrate that disorder can act to freeze only the lowest-energy magnetic degrees of freedom; at higher energies, a magnetic excitation continuum characteristic of fractionalized excitations persists.

The existence of a spin liquid for isotropically interacting classical spins on the pyrochlore lattice was first proposed by Jacques Villain nearly 40 years ago[1]. Since then, it has been established that the classical ($S \rightarrow \infty$) Heisenberg antiferromagnet does not undergo any magnetic ordering transition[2–6]. The magnetic interaction energy is minimized by all spin configurations with vanishing magnetization on every tetrahedron, and the ensemble of these configurations forms a macroscopically degenerate, but highly correlated, ground-state manifold. Such a collective state is termed a Coulomb phase because coarse-grained spin configurations within the manifold form a divergence-free vector field, implying dipolar correlations[7–9]. Experiments probing magnetic correlations, and hence the solenoidal field, should include sharp pinch point features, as in related classical spin-ice materials, where ferromagnetic Ising interactions dominate[10]. Both classical spin ice and the classical Heisenberg antiferromagnet may be classified as Coulomb phases but, whereas there is much activity and progress in exploring quantum spin ice, less is understood about the quantum limit of the antiferromagnetic Heisenberg model. There is theoretical evidence that pinch point correlations survive[2,3,11–13], but the specific character of the ground state and of the magnetic excitations is unknown.

The experimental challenge lies in realizing the pyrochlore Heisenberg model in a material. The highly degenerate manifold of the Coulomb phase is susceptible to small perturbations[2] and lattice instabilities[14] such that at low temperatures the spin liquid phase is more often than not supplanted by a broken-symmetry phase. So far, the closest realizations of a Heisenberg antiferromagnet on a pyrochlore lattice have been found in the cubic spinels. Many of these materials exhibit considerable exchange interactions extending to the second- and third-nearest neighbours[15]. Magnetic frustration is manifest through self-organized independent hexagonal clusters[16–19], but a magneto-structural transition severely impacts almost half of the magnetic bandwidth.

Extrinsic disorder, in the form of impurity ions, or variations in magnetic exchange interactions caused by chemical disorder may also disrupt the spin liquid. Generally, these perturbations result in a spin-freezing transition at low temperatures[20–22]. For example, in the Heisenberg pyrochlore $Y_2Mo_2O_7$, weak disorder results in a fully frozen state with isotropic short-range spin correlations[23,24]. Here, we demonstrate that disorder is not necessarily fatal to the search for quantum spin liquids, as it can act to freeze only the lowest energy magnetic degrees of freedom. At higher energies a magnetic excitation continuum characteristic of fractionalized excitations persists.

$NaCaNi_2F_7$ is one member of a family of recently discovered transition metal pyrochlore fluorides where charge balance in the neutral chemical structure requires an equal mixture of Na^{1+} and Ca^{2+} (refs [25–27]). Diffraction measurements probing the average crystal structure indicate that Na^{1+} and Ca^{2+} are uniformly and randomly distributed on the

A-site of the pyrochlore lattice. Magnetic susceptibility measurements reveal Curie–Weiss behaviour, with an effective moment of $p_{eff} = 3.7(1)\mu_B$ (where μ_B is the Bohr magneton), consistent with $S = 1$, and a Curie–Weiss temperature of $\theta_{CW} = 129(1)$ K (ref. [26]). A spin-glass-like freezing transition is observed at $T_f = 3.6$ K in d.c. and a.c. magnetic susceptibility measurements[26]. This freezing may result from the Na^{1+}/Ca^{2+} charge disorder, which is expected to generate a random variation in the magnetic exchange interactions. For the Heisenberg pyrochlore antiferromagnet described by the Hamiltonian $\mathscr{H} = 1/2\sum_{ij} J_{ij}\mathbf{S}_i \cdot \mathbf{S}_j$ the freezing temperature provides an estimate[21] of the strength of the bond disorder $\delta J = \sqrt{3/8}\, k_B T_f = 0.19$ meV for $S = 1$. Despite this disorder, for temperatures (T) and energies E beyond 2% of the magnetic bandwidth, we show that $NaCaNi_2F_7$ is an excellent approximation to a nearest-neighbour Heisenberg antiferromagnet on the pyrochlore lattice, and exhibits key characteristics of a quantum spin liquid (QSL): an excitation continuum and a finite energy maximum in the momentum-resolved spectrum of scattering at an energy transfer of the order of the nearest-neighbour exchange constant.

We start by determining the spin Hamiltonian for $NaCaNi_2F_7$. The elegant method employed for other frustrated magnets[28,29] is not feasible here because the magnetic energy scale is too large to reach the forced ferromagnetic state in a neutron scattering experiment. Instead we focus on the equal-time spin correlation function, which can be measured with inelastic neutron scattering and calculated for a given spin Hamiltonian in the paramagnetic state through the self-consistent Gaussian approximation (SCGA)[15]. Fig. 1a shows the measured equal-time structure factor $\mathcal{S}(q)$ for $NaCaNi_2F_7$ obtained from the energy-integrated magnetic neutron scattering intensity. More detailed information is provided by polarized neutron scattering in the (h, h, ℓ) plane, which is sensitive to spin components perpendicular to $\mathbf{q}$ within the (h, h, ℓ) reciprocal lattice plane for the spin-flip (SF) channel, and along $(1,-1,0)$ for the non-spin-flip channel (NSF). Without further analysis, the similarity of SF and NSF magnetic neutron intensities in Fig. 1a is evidence of a near spin-space isotropic system. Weak anisotropic interactions are revealed by two features of the polarized intensity. First, the SF scattering exhibits a pronounced asymmetry of the lobes of intensity centred on $(\pm 0.6, \pm 0.5, 2)$ positions about the dashed line parallel to $(1,1,0)$ and passing though $(0, 0, 2)$, as indicated in Fig. 1b. Second, the NSF intensity is diminished around the $(0, 0, 2)$ pinch point positions.

The full symmetry-allowed nearest-neighbour bilinear exchange Hamiltonian takes the form $\mathscr{H} = 1/2\sum_{ij} J_{ij}^{\mu\nu} S_i^\mu S_j^\nu$, where the 3×3 interaction matrix $J^{\mu\nu}$ is parameterized by four independent terms: the diagonal components J_1 and J_2, and off-diagonal components J_3 and J_4 (ref. [29]). For the next-nearest-neighbour interactions J_{NNN} we retain only the isotropic part. We find the best global fit of the measured equal-time structure factor with the SCGA using the exchange parameters: $J_1 = J_2 = 3.2(1)$ meV, $J_3 = 0.019(3)$ meV, $J_4 = -0.070(4)$ meV and $J_{NNN} = -0.025(5)$ meV. Details of the neutron measurements, fitting procedure and the goodness of fit diagnostics are provided in the Methods and Supplementary Information. The resulting calculated neutron intensity is shown in Fig. 1b. Although the SCGA is an approximate procedure, we find exceptional agreement between the model and data, and we shall later see that a classical Monte Carlo calculation of the specific heat based on

the inferred spin Hamiltonian is consistent with our measurements. Although the effective moment of 3.7(1) μ_B implies an orbital contribution to the magnetism[26], we find that the effect of spin-orbit coupling on the exchange Hamiltonian is very small. We conclude that the spin Hamiltonian for $NaCaNi_2F_7$ closely approximates the $S = 1$ Heisenberg antiferromagnet on the pyrochlore lattice, perturbed only at the percent level by symmetric and antisymmetric exchange anisotropies, next-nearest-neighbour interactions and exchange disorder.

Having established its frustrated quantum spin Hamiltonian, we now explore the corresponding magnetic excitations in $NaCaNi_2F_7$. Figure 2 shows the **q**-dependence of the inelastic magnetic scattering through a series of constant-energy transfer slices covering the (h, h, ℓ) and $(h, 0, \ell)$ reciprocal lattice planes. At low energy transfer, the dynamic structure factor forms a bow-tie pattern with pinch points characteristic of dipolar spin correlations. The scattering closely resembles predictions for the classical Heisenberg antiferromagnet on the pyrochlore lattice[7,8,15], but with important deviations, including a slight momentum broadening and reduction of intensity around the pinch points. For $E = 8$ meV the magnetic scattering extends through more of momentum space with subtle modulations in intensity, particularly near $(-2, -2, 0)$ in the (h, h, ℓ) zone, where a double-ridge structure resembles highly damped dispersing spin waves in a one-dimensional magnet. Sharper features around $(-2, -2, 2)$ and at high **q** arise from phonon scattering. Finally, at $E = 11$ meV magnetic scattering is uniformly distributed through momentum space, except for exclusion zones centred around the Γ point, where scattering is precluded for a Heisenberg model[30].

In Fig. 3 we present the momentum- and energy-resolved spin-flip neutron scattering cross-section. For our experiment this cross-section is sensitive only to magnetic scattering and nuclear incoherent scattering; thus data in Fig. 3 are representative of the dynamic structure factor uncontaminated by coherent non-magnetic scattering. The magnetic excitations form a continuum that extends over an energy bandwidth of ~12.5 meV ~$4JS_1$. Along the $(h, h, 2)$ direction and pinch point ridge, the inelastic neutron intensity is relatively featureless. However, along the $(2, 2, \ell)$ direction, which traverses the pinch point ridge, the magnetic scattering is more structured, becoming doubly peaked above 5 meV. This precludes factorization of the dynamic structure factor: $\mathcal{S}(\mathbf{q}, E) \neq \mathcal{S}(\mathbf{q})f(E)$, which distinguishes $NaCaNi_2F_7$ from the classical limit of the Heisenberg model on the pyrochlore lattice[31]. In the constant-momentum and constant-energy transfer cuts plotted in Fig. 3b,c very broad dispersive ridges are observed. Whereas the spectrum is gapless down to the 0.17 meV scale set by our finest energy resolution measurements, the dynamic structure factor is peaked at finite energy transfers and can be fitted with the spectral form of an over-damped harmonic oscillator. The characteristic energy scale disperses from $E_q = 4.8$ meV~J_1 at the pinch point $\mathbf{q} = (2, 2, 0)$, to $E_q = 7.8$ meV at the nodal point $\mathbf{q} = (2, 2, 1)$. This spectrum distinguishes $NaCaNi_2F_7$ from recent theoretical treatments of the semiclassical Heisenberg model, which find a purely diffusive response that is peaked at zero energy[13]. The absence of inelastic scattering at the Γ point and our polarized neutron measurements rule out any sizeable single-ion anisotropies that could explain the peak in spectral weight at non-zero energy transfers. The only energy scale large enough to account for the resonance is the nearest-neighbour antiferromagnetic exchange interaction J_1.

A conservative interpretation is that the dispersing modes are overdamped spin waves of an underlying classical magnetic order, disrupted in $NaCaNi_2F_7$ by exchange disorder. Since the frozen spin configurations feature non-collinear interacting spins, single-particle $S = 1$ magnon excitations can decay from interactions with multimagnon states to form a continuum of scattering[32]. Such a scenario may be appropriate for the related pyrochlore XY antiferromagnet $NaCaCo_2F_7$[25]. Elastic magnetic neutron scattering from $NaCaCo_2F_7$ resembles that of an ordered antiferromagnet, consistent with the non-collinear magnetic structure favoured by an order-by-disorder mechanism[33]. This order develops at a temperature coincident with a broad peak in the magnetic specific heat, which constitutes the total magnetic entropy of the $J = 1/2$ magnetic moments formed by Co ions. The fraction of elastic magnetic neutron intensity for $NaCaCo_2F_7$ is 0.3(1)[33], almost exactly as expected for an ordered $S = 1/2$ magnet ($S^2/S(S + 1) = 1/3$). Thus, it appears that in $NaCaCo_2F_7$, exchange disorder truncates the magnetic correlations of the classical antiferromagnetic order favoured by the underlying Hamiltonian.

In contrast, for $NaCaNi_2F_7$, by comparing the spectral weight for elastic ($E < 0.7$ meV) and inelastic scattering ($0.7 < E < 14$ meV) we find ~90% of the magnetic scattering is inelastic in the low-T limit. This greatly exceeds the 50% mark for a semi-classical ground state based on $S = 1$ Ni ions, and is direct evidence of a spin system dominated by quantum fluctuations. Integrating the data for the dynamic spin correlation function $\mathcal{S}(\mathbf{q}, E)$ over momentum and energy, including the elastic diffuse magnetic scattering, we recover the total spectral weight of $3 \int S(\mathbf{q}, E) \mathrm{d}E \, \mathrm{d}^3q = 13(1)$, which is consistent with the $(3.7\mu_B)^2 = 13.7\mu_B^2$ effective moment extracted from the high-T magnetic susceptibility data[26].

The magnetic specific heat $C_m(T)$ (Fig. 4a) provides an excellent overview of three distinct regimes of magnetism in $NaCaNi_2F_7$. For > 18 K, $C_m(T)$ follows the form expected for the classical spin liquid (Villain's cooperative paramagnet) phase of the Heisenberg antiferromagnet on a pyrochlore lattice. The dashed line in Fig. 4a shows that a classical Monte Carlo simulation of the Heisenberg model with the exchange parameters extracted from neutron scattering provides an excellent account of the data.

In the second regime, where $T \sim J_1$, as indicated by light shading in Fig. 4a, $C_m(T)$ falls below the classical model. The corresponding broad maximum at 18 K thus marks the crossover from classical to quantum spin liquid. Finally, for $< T_f = 3.6$ K, a discontinuity in $\mathrm{d}_m(T)/\mathrm{d}T$ (inset of Fig. 4a) indicates spin freezing[26]. A fit to $C_m(T) \propto T^\alpha$ for $T < T_f$ yields $\alpha = 2.2(1)$. $C_m \propto T^2$ has been found for $T < T_f$ in a number of frustrated magnets with spin-disordered ground states[24,34,35]. This form can arise from linearly dispersing bosonic quasi-particles in two dimensions. Although this might seem out of place for cubic $NaCaNi_2F_7$, frustration can produce soft 'nodal' lines which effectively reduce dimensionality to two[36]. The lack of translational symmetry in $NaCaNi_2F_7$ implies the corresponding quasi-particles cannot manifest as coherent modes in neutron scattering, yet $C_m(T)$ reflects their density of states[37,38].

In Fig. 4b we show the magnetic entropy recovered between 100 mK and 150 K that saturates at 84% of the available $R\ln(3)$ for $S = 1$. We interpret the $0.176R$ per spin residual

entropy at 100 mK as indicating broken ergodicity for $T < T_f$. Specifically, we propose that below T_f a metastable spin configuration within the Coulomb phase manifold is kinetically arrested by the disorder potential so the material no longer explores all states of a given energy. Correspondingly, we expect spin correlations for $E < k_B T_f$ to reflect a disorder-dominated regime. Figure 4d shows the onset of elastic neutron scattering for < 8 K. In a continuation of the trend in a.c.-susceptibility data[26], the apparent freezing temperature increases with the measurement frequency, which here is the energy resolution of $\Delta E = 0.37$ meV. The momentum width of the elastic signal is independent of T, indicating the sample averaged spatial correlations are unaffected by the freezing transition. Figure 4c shows the elastic magnetic neutron scattering in two high-symmetry reciprocal lattice planes of the cubic lattice. The signal is dominated by extended diffuse intensity arising from short-range correlated spin configurations that are static within the 10 ps time window of our measurement. Neutron intensity is concentrated in lobes centred near $\mathbf{q} = (2n \pm 0.6,\ 2n \pm 0.6,\ 0)$ positions, where n is an integer. Near (002) and (220), where sharp pinch point features representing long-range dipolar correlations of the pure Heisenberg model are expected, the momentum distribution of the scattering is broader than the experimental resolution. The inverse momentum width corresponds to a real-space correlation length of $\xi = 6$ Å, or just two nearest-neighbour lattice spacings.

By averaging the elastic ($E = 0$) intensity over the accessible parts of the Brillouin zone we find the frozen moment accounts for only $|\langle \mathbf{S} \rangle|/S = 44\%$ of the saturation magnetization for Ni^{2+}. The small fraction of frozen magnetization is similar to that of the spin- 3/2 kagome lattice $KCr_3(OD)_6(SO_4)_2$ (ref. [39]). To gain insight into the nature of this unconventional frozen low-temperature state, we have carried out classical Monte Carlo simulations of the Heisenberg Hamiltonian relevant to $NaCaNi_2F_7$. Random bond disorder was included by sampling from a box distribution, with a half-width of $\delta J = 0.19$ meV and exchange parameters extracted from an independent analysis of inelastic neutron scattering data. In Fig. 4c we compare the measured elastic scattering with the corresponding numerically modelled signal. The overall qualitative agreement gives confidence in our optimized magnetic Hamiltonian and numerical simulations.

A number of theoretical investigations[2,15,40–42] have shown that small perturbations in the classical Heisenberg model, J', in the form of exchange anisotropies or further-neighbour interactions, result in a magnetically ordered phase below temperatures of the order of J' S^2. In $NaCaNi_2F_7$ these perturbations are significantly smaller than the freezing temperature. Correspondingly, our Monte Carlo simulations for the anisotropic Hamiltonian relevant to $NaCaNi_2F_7$, but without exchange disorder, find no classical magnetic order above $T = 500$ mK. So even if the disorder free spin-Hamiltonian for $NaCaNi_2F_7$ ultimately has long-range magnetic order, it is preempted by exchange-disorder-induced spin freezing.

The spin configurations generated through Monte Carlo simulation offer a unique real-space view of frozen magnetism in $NaCaNi_2F_7$. In the absence of disorder, the energy of the classical Heisenberg Hamiltonian is minimized by all states with zero total spin per tetrahedra, $\mathbf{S}_{tot} = \sum_{i=1}^{4} \mathbf{S}_i = 0$. We find the lowest energy states for the bond-disordered Heisenberg Hamiltonian with small anisotropic exchanges relevant to $NaCaNi_2F_7$ also fall

approximately within the $\mathbf{S}_{tot} = 0$ manifold (see Supplementary Information). This manifold is parameterized by the order parameters $f_1 = [(\mathbf{S}_1 + \mathbf{S}_2) \cdot (\mathbf{S}_3 + \mathbf{S}_4) - 2\mathbf{S}_1 \cdot \mathbf{S}_2 - 2\mathbf{S}_3 \cdot \mathbf{S}_4]/\sqrt{12}$ and $f_2 = (\mathbf{S}_1 \cdot \mathbf{S}_3 + \mathbf{S}_2 \cdot \mathbf{S}_4 - \mathbf{S}_2 \cdot \mathbf{S}_3 - \mathbf{S}_1 \cdot \mathbf{S}_4)/2$ refs [14,42]). The statistical distribution of f_1 and f_2 over a Monte Carlo ensemble of tetrahedra provides a local characterization of the particular frozen $\mathbf{S}_{tot} = 0$ spin configuration. Such histograms of (f_1, f_2) extracted from our Monte Carlo simulations are shown in Fig. 4e, where possible values span an equilateral triangle in the (f_1, f_2) plane. Tetrahedra with pairs of antiparallel spins lie along the triangular edges and collinear spin configurations are at the vertices. The classical Heisenberg (only) model with weak bond disorder is glassy[21], with a tendency to form locally collinear states; this is confirmed by the results in the top half of Fig. 4e (ref. [20]) The enhanced density along the boundaries, and away from the corners, of the lower part of the triangle in Fig. 4e indicates a tendency to form configurations of pairwise collinear spins when the small anisotropic interactions specific to $NaCaNi_2F_7$ are added.

Let us now discuss the fundamental challenges presented by our results on $NaCaNi_2F_7$. We have shown this three-dimensional spin-1 system forms a nearly spin-space-isotropic Coulomb-like phase, with vanishing net spin on each of the corner-sharing tetrahedra and a broad gapless continuum of spin-flip excitations. Because we are dealing with a crystalline solid at low temperatures, this implies the absence of propagating magnons and a spin system that either has no quasi-particles or where the quasi-particles are inaccessible to neutron scattering.

Whereas conventional spin wave theory is built upon a spin-ordered ground state, $NaCaNi_2F_7$ has a low-energy manifold distinguished by local constraints that do not impose a unique ordered state. There is weak exchange disorder and a non-ergodic aperiodic frozen component, but these features cannot have major impacts at high energies because of the discrepancy in energy scales ($\delta J/J \approx 6\%$). More detrimental to a spin wave picture are the local soft modes that characterize corner-sharing simplexes such as the kagome, and here the pyrochlore lattice. These present scattering centres for putative magnons, which correspondingly become overdamped and lose their quasi-particle status. The broad dispersing ridges that we do observe in the $\mathbf{q} - E$ dependence of the magnetic neutron scattering cross-section (Fig. 3) might loosely be associated with such incoherent magnons.

The efficacy of a semi-classical spin wave expansion to describe quantum spin systems with incoherent magnons is, however, questionable. Specifically, quantum tunnelling may be important in describing local soft modes for $S = 1$, and this could impact both the spectrum of excitations and the nature of the ground state. Considering, furthermore, that 90% of the magnetic spectral weight for $NaCaNi_2F_7$ lies in the inelastic channel, a description of its magnetism in terms of a quantum spin liquid may be more appropriate. For energies above $k_B T_f$, the continuous spectrum is consistent with the fractionalization of a spin-flip excitation into weakly interacting multiparticle excitations. The non-ergodic regime for energies below $k_B T_f$ might be associated with the pinning of these fractionalized excitations by exchange disorder. A quantitative measure of the frozen subspace is provided by the fraction of the total entropy that is residual ($\Delta S/R\ln(3) = 16(4)\%$) which is within error bars of the fraction of the total spectral weight contained in elastic scattering ($\langle m_{elastic}\rangle^2/(g^2 S(S+1)) = 10(2)\%$).

Our experiments on $NaCaNi_2F_7$ show frustration and weak disorder can completely suppress conventional spin order in three dimensions, leaving behind strong spin-1 quantum fluctuations at low temperatures. The quantitative spin Hamiltonian that we have developed, and the distinct collective properties that we have documented, establish $NaCaNi_2F_7$ as an ideal model system for what would appear to be a new state of matter.

Methods

The identification of any commercial product or trade name does not imply endorsement or recommendation by the National Institute of Standards and Technology.

Specific heat.

Heat capacity measurements were conducted using a Quantum Design PPMS with a dilution insert for temperatures between 100 mK and 4 K, and standard insert for temperatures between 2 K and 270 K. All measurements were carried out on the same 5 mg single crystal using the adiabatic pulse method. The non-magnetic contribution over the full measured temperature range was determined by scaling the measured specific heat of the iso-structural compound $NaCaZn_2F_7$ by the relative Debye temperatures.

Neutron scattering.

All neutron scattering measurements were performed on the same 3 g single crystal, grown as described elsewhere[26]. Unpolarized neutron scattering measurements were performed on the MACS spectrometer[44] at the NIST Center for Neutron Research. Neutron momentum transfer is indexed in the cubic lattice with $a^* = 2\pi/a = 0.61 \text{ Å}^{-1}$. Measurements were performed with the sample oriented in both the (h, h, ℓ) and $(h, k, 0)$ scattering planes. For elastic $(E = 0)$ measurements the monochromator was configured in a vertical focusing configuration for a neutron energy of 5 meV. Two configurations were used for inelastic measurements, both with the monochromator in double-focusing mode. For energy transfers below 1.4 meV, MACS was operated with a fixed final energy of 3.7 meV and with Be and BeO filters before and after the sample, respectively. For energy transfers above 1.4 meV we used a fixed final energy of 5 meV with a Be filter after the sample and no incident beam filter. Data for energy transfers above 1.4 meV were corrected for the effects of contamination from high-order harmonics in the incident beam neutron monitor.

Polarized neutron scattering measurements were carried out on the HYSPEC spectrometer[45] at the Spallation Neutron Source at Oak Ridge National Lab. An incident neutron energy of 17 meV was selected using a Fermi chopper rotating at 240 Hz, resulting in an energy resolution of $\delta E = 1.4$ meV for the elastic line. The incident neutron beam polarization was defined using a vertically focusing Heusler monochromator, while the outgoing beam polarization was selected using a radially collimating supermirror array. All polarized measurements were performed with the guide field applied perpendicular to the (h, h, l) scattering plane, along the $(1, -1, 0)$ direction. In this configuration, SF scattering measures the component of magnetic cross-section that is polarized within the scattering plane and perpendicular to **q**, whereas NSF measures the out-of-plane component, here along the (1,

−1,0) direction. The flipping ratio measured on a (4, 4, 0) nuclear Bragg peak was 16. All data reduction and analysis was carried out using the Mantid software suite[46].

Quantitative measurement of the energy- and momentum-resolved magnetic neutron cross-section in $NaCaNi_2F_7$ was essential for a detailed comparison of neutron scattering and specific heat data. To accurately distinguish magnetic scattering intensity, both unpolarized and polarized measurements were performed. Measured neutron count rates from both instruments were converted into absolute units of the neutron scattering cross-section using incoherent elastic scattering from the sample as a reference scattering cross-section. The scale factor for conversion to absolute units was additionally cross-checked against measurements from a vanadium standard.

Numerical methods.

We fit the static structure factor from the neutron scattering data to the corresponding prediction of the self-consistent Gaussian approximation (SCGA) at 1.8 K, to obtain the magnetic interaction parameters in the main text. Details of the method, including the cost function and error analysis, are discussed in the Supplementary Information. The results of the SCGA are complemented by classical Monte Carlo calculations, from which we extract both the specific heat and the magnetic structure factor. Monte Carlo simulations used single spin updates for continuous spin on pyrochlore lattices (with 16-site cubic unit cells) of size $N = 16L^3$ for $L = 3$ to $L = 10$. To determine the classical ground state of the fitted spin Hamiltonian, parallel tempering Monte Carlo[47] was carried out with $T_{min} = 0.01$ K and $T_{max} = 1$ K with the number of replicas $N_r = \sqrt{N}\ln(T_{max}/T_{min})$ (approximately 100 for $L = 3$ and 400 for $L = 8$, the two sizes studied extensively, see Supplementary Information for more analyses) and the simulation carried out for a total of 10^8 steps. With the lowest-energy configurations encountered in this finite Monte Carlo run, further iterative minimization was performed to accelerate the approach to the classical ground state. For these optimized spin configurations (many of which are local minima), two-component local order parameters (f_1 and f_2) are calculated on all $N/4$ tetrahedra of a fixed orientation ('up'). This was repeated for 50–100 bond-disorder realizations and the combined data set, including all tetrahedra and disorder realizations, was used to obtain the two-dimensional histogram in Fig. 4. The static structure factor from these low-energy, zero-temperature configurations, for $L = 8$, was averaged to obtain an estimate of the elastic neutron cross-section. Further details of all methods and algorithms employed are provided in the Supplementary Information.

Supplementary Material

Refer to Web version on PubMed Central for supplementary material.

Acknowledgements

Data availability

The data that support the plots within this paper and other findings of this study are available from the corresponding author upon reasonable request.

References

1. Villain J Insulating spin glasses. Z. Phys. B 33, 31–42 (1979).

2. Harris AB, Berlinsky AJ & Bruder C Ordering by quantum fluctuations in a strongly frustrated Heisenberg antiferromagnet. J. Appl. Phys. 69, 5200–5202 (1991).

3. Canals B & Lacroix C Pyrochlore antiferromagnet: A three-dimensional quantum spin liquid. Phys. Rev. Lett. 80, 2933–2936 (1998).

4. Canals B & Lacroix C Quantum spin liquid: The Heisenberg antiferromagnet on the three-dimensional pyrochlore lattice. Phys. Rev. B 61, 1149–1159 (2000).

5. Moessner R & Chalker JT Properties of a classical spin liquid: The Heisenberg pyrochlore antiferromagnet. Phys. Rev. Lett. 80, 2929–2932 (1998).

6. Moessner R & Chalker JT Low-temperature properties of classical geometrically frustrated antiferromagnets. Phys. Rev. B 58, 12049–12062 (1998).

7. Isakov SV, Gregor K, Moessner R & Sondhi SL Dipolar spin correlations in classical pyrochlore magnets. Phys. Rev. Lett. 93, 167204 (2004). [PubMed: 15525027]

8. Henley CL Power-law spin correlations in pyrochlore antiferromagnets. Phys. Rev. B 71, 014424 (2005).

9. Henley CL The Coulomb phase in frustrated systems. Annu. Rev. Condens. Matter Phys. 1, 179–210 (2010).

10. Fennell T et al. Magnetic Coulomb phase in the spin ice $Ho_2Ti_2O_7$. Science 326, 415–417 (2009). [PubMed: 19729619]

11. Isoda M & Mori S Valence-bond crystal and anisotropic excitation spectrum on 3-dimensionally frustrated pyrochlore. J. Phys. Soc. Jpn 67, 4022–4025 (1998).

12. Moessner R, Sondhi SL & Goerbig MO Quantum dimer models and effective Hamiltonians on the pyrochlore lattice. Phys. Rev. B 73, 094430 (2006).

13. Huang Y, Chen K, Deng Y, Prokof'ev N & Svistunov B Spin-ice state of the quantum Heisenberg antiferromagnet on the pyrochlore lattice. Phys. Rev. Lett. 116, 177203 (2016). [PubMed: 27176537]

14. Tchernyshyov O, Moessner R & Sondhi SL Order by distortion and string modes in pyrochlore antiferromagnets. Phys. Rev. Lett. 88, 067203 (2002). [PubMed: 11863847]

15. Conlon PH & Chalker JT Absent pinch points and emergent clusters: Further neighbor interactions in the pyrochlore Heisenberg antiferromagnet. Phys. Rev. B 81, 224413 (2010).

16. Lee S-H et al. Emergent excitations in a geometrically frustrated magnet. Nature 418, 856–858 (2002). [PubMed: 12192404]

17. Kamazawa K, Park S, Lee S-H, Sato TJ & Tsunoda Y Dissociation of spin objects in geometrically frustrated $CdFe_2O_4$. Phys. Rev. B 70, 024418 (2004).

18. Chung J-H et al. Statics and dynamics of incommensurate spin order in a geometrically frustrated antiferromagnet $CdCr_2O_4$. Phys. Rev. Lett. 95, 247204 (2005). [PubMed: 16384420]

19. Tomiyasu K et al. Molecular spin resonance in the geometrically frustrated magnet $MgCr_2O_4$ by inelastic neutron scattering. Phys. Rev. Lett. 101, 177401 (2008). [PubMed: 18999783]

20. Bellier-Castella L, Gingras MJP, Holdsworth PCW & Moessner R Frustrated order by disorder: The pyrochlore anti-ferromagnet with bond disorder. Can. J. Phys. 79, 1365–1371 (2001).

21. Saunders TE & Chalker JT Spin freezing in geometrically frustrated antiferromagnets with weak disorder. Phys. Rev. Lett. 98, 157201 (2007). [PubMed: 17501375]

22. Sen Arnab & Moessner, R. Topological spin glass in diluted spin ice. Phys. Rev. Lett. 114, 247207 (2015). [PubMed: 26197007]

23. Gardner JS et al. Glassy statics and dynamics in the chemically ordered pyrochlore antiferromagnet $Y_2Mo_2O_7$. Phys. Rev. Lett. 83, 211–214 (1999).

24. Silverstein HJ et al. Liquidlike correlations in single-crystalline $Y_2Mo_2O_7$: An unconventional spin glass. Phys. Rev. B 89, 054433 (2014).

25. Krizan JW & Cava RJ $NaCaCo_2F_7$: A single-crystal high-temperature pyrochlore antiferromagnet. Phys. Rev. B 89, 214401 (2014).

26. Krizan JW & Cava RJ $NaCaNi_2F_7$: A frustrated high-temperature pyrochlore antiferromagnet with $S = 1$ Ni^{2+}. Phys. Rev. B 92, 014406 (2015).

27. Sanders MB, Krizan JW, Plumb KW, McQueen TM & Cava RJ $NaSrMn_2F_7$, $NaCaFe_2F_7$, and $NaSrFe_2F_7$: novel single crystal pyrochlore antiferromagnets. J. Phys. Condens. Matter 29, 045801 (2017). [PubMed: 27875333]

28. Coldea R et al. Direct measurement of the spin Hamiltonian and observation of condensation of magnons in the 2d frustrated quantum magnet Cs_2CuCl_4. Phys. Rev. Lett. 88, 137203 (2002). [PubMed: 11955122]

29. Ross KA, Savary L, Gaulin BD & Balents L Quantum excitations in quantum spin ice. Phys. Rev. X 1, 021002 (2011).

30. Hohenberg PC & Brinkman WF Sum rules for the frequency spectrum of linear magnetic chains. Phys. Rev. B 10, 128–131 (1974).

31. Conlon PH & Chalker JT Spin dynamics in pyrochlore Heisenberg antiferromagnets. Phys. Rev. Lett. 102, 237206 (2009). [PubMed: 19658970]

32. Zhitomirsky ME & Chernyshev AL Colloquium: Spontaneous magnon decays. Rev. Mod. Phys. 85, 219–242 (2013).

33. Ross KA, Krizan JW, Rodriguez-Rivera JA, Cava RJ & Broholm CL Static and dynamic *XY*-like short-range order in a frustrated magnet with exchange disorder. Phys. Rev. B 93, 014433 (2016).

34. Ramirez AP, Hessen B & Winklemann M Entropy balance and evidence for local spin singlets in a kagome-like magnet. Phys. Rev. Lett. 84, 2957–2960 (2000). [PubMed: 11018985]

35. Nakatsuji S et al. Spin disorder on a triangular lattice. Science 309, 1697–1700 (2005). [PubMed: 16151004]

36. Bergman D, Alicea J, Gull E, Trebst S & Balents L Order-by-disorder and spiral spin-liquid in frustrated diamond-lattice antiferromagnets. Nat. Phys. 3, 487–491 (2007).

37. Halperin BI & Saslow WM Hydrodynamic theory of spin waves in spin glasses and other systems with noncollinear spin orientations. Phys. Rev. B 16, 2154–2162 (1977).

38. Podolsky D & Kim YB Halperin–Saslow modes as the origin of the low-temperature anomaly in $NiGa_2S_4$. Phys. Rev. B 79, 140402 (2009).

39. Lee S-H et al. Less than 50% sublattice polarization in an insulating S = 3/2 kagome antiferromagnet at T ≈ 0. Phys. Rev. B 56, 8091–8097 (1997).

40. Reimers JN, Berlinsky AJ & Shi A-C Mean-field approach to magnetic ordering in highly frustrated pyrochlores. Phys. Rev. B 43, 865–878 (1991).

41. Elhajal M, Canals B, Sunyer R & Lacroix C Ordering in the pyrochlore antiferromagnet due to Dzyaloshinsky–Moriya interactions. Phys. Rev. B 71, 094420 (2005).

42. Chern G-W, Moessner R & Tchernyshyov O Partial order from disorder in a classical pyrochlore antiferromagnet. Phys. Rev. B 78, 144418 (2008).

43. Brown PJ International Tables for Crystallography (ed. Prince E.) 454–461 (Springer, Berlin, 2006).

44. Rodriguez JA et al. MACS a new high intensity cold neutron spectrometer at NIST. Meas. Sci. Technol. 19, 034023 (2008).

45. Zaliznyak IA et al. Polarized neutron scattering on HYSPEC: the hybrid spectrometer at SNS. J. Phys. Conf. Ser. 862, 012030 (2017).

46. Arnold O et al. Mantid—Data analysis and visualization package for neutron scattering and μSR experiments. Nucl. Instrum. Methods Phys. Res. A 764, 156–166 (2014).

47. Hukushima K & Nemoto K Exchange Monte Carlo method and application to spin glass simulations. J. Phys. Soc. Jpn 65, 1604–1608 (1996).
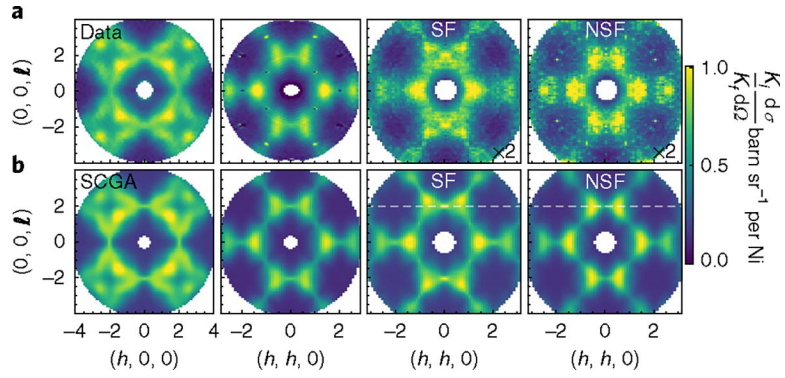
Fig. 1 |. Equal-time structure factor in NaCaNi$_2$F$_7$.
a, Measured neutron cross-section integrated over the range $0 < E < 14$ meV at $T = 1.8(2)$ K.
Polarized neutron measurements are labelled by NSF, which measures components of
the dynamic spin correlation function that are perpendicular to the (h, h, ℓ) scattering
plane, and SF, which measures the component of the dynamics spin correlation function
polarized within the (h, h, ℓ) scattering plane and perpendicular to momentum transfer.
Before integration, the data were symmetrized by folding about the lines $h = 0$ and $\ell = 0$ for
data in the $(h, 0, \ell)$ scattering plane and the lines $hh = 0$ and $\ell = 0$ for data in the (h, h, ℓ)
scattering plane. No smoothing or interpolation was applied to the data. **b**, Energy-integrated
neutron cross-section calculated using the self-consistent Gaussian approximation (SCGA)
and exchange parameters $J_1 = J_2 = 3.2(1)$ meV, $J_3 = 0.019(3)$ meV $J_4 = -0.070(4)$ meV and
$J_{\mathrm{NNN}} = -0.025(5)$ meV. Dashed lines delineate the plane of asymmetry in the SF scattering.
The dipole approximation for the Ni^{2+} magnetic form factor[43] was used when converting the
calculated $\mathcal{S}(\mathrm{q})$ to a neutron cross-section.
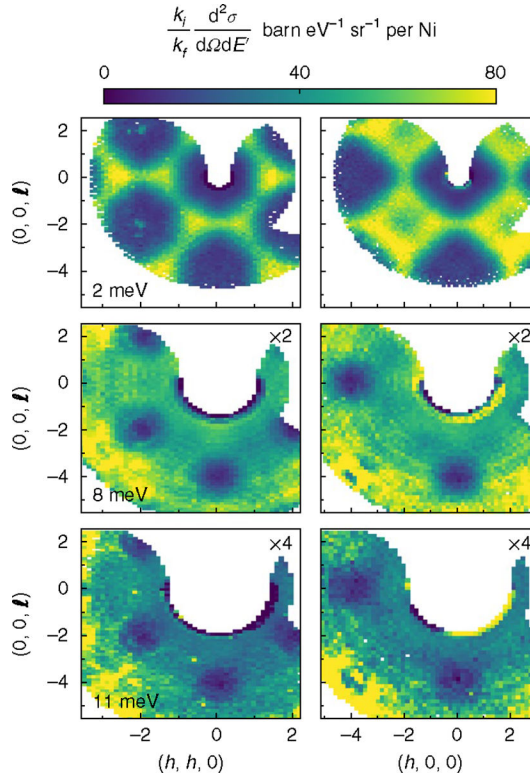
Fig. 2 |. Inelastic neutron scattering showing dynamic magnetic correlations in NaCaNi$_2$F$_7$.
Momentum and energy dependence of inelastic magnetic scattering in NaCaNi$_2$F$_7$ for the (h, h, ℓ) and $(h, k, 0)$ scattering planes at = 1.8 K. Each slice was integrated over an energy transfer range of ± 0.25 meV. No smoothing or symmetrization was applied to the data. Above energy transfers of 0.5 meV, the dynamic magnetic correlations form a 'bow-tie' pattern in momentum space. The sharp pinch-point-like features around (2, 0, 0) and (2, 2, 0) positions indicate that the net magnetization per tetrahedron vanishes in the Coulomb-like phase realized in NaCaNi$_2$F$_7$. Above energies of 5 meV, the scattering forms a broad continuum with no intensity around the Γ points.
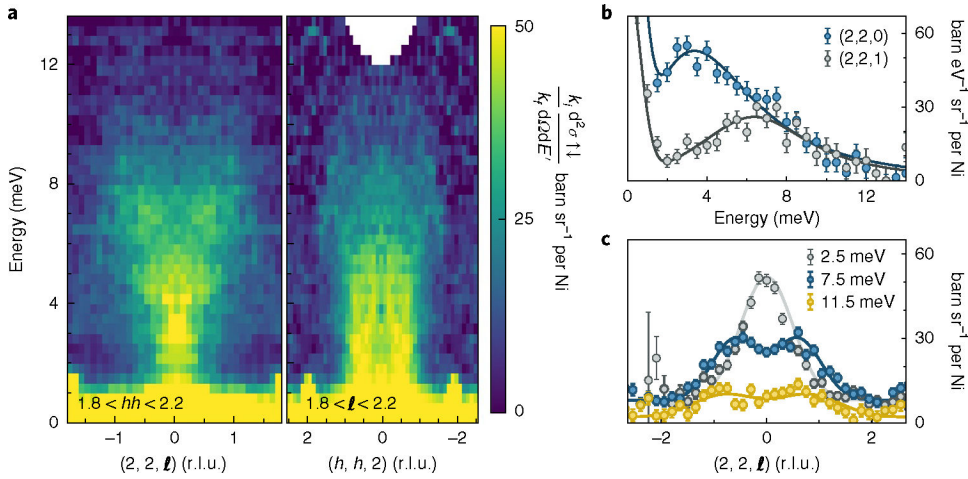
Fig. 3 |. Momentum- and energy-resolved inelastic neutron scattering probing magnetic excitations in NaCaNi$_2$F$_7$.

a, Energy-momentum slices through the spin-flip portion of the polarized neutron scattering cross-section at = 1.8 K. The data were symmetrized by folding about the line along $(0, 0, \ell)$ for the $(2, 2, \ell)$-energy slice and the line along $(h, h, 0)$ for the $(h, h, 2)$-energy slice. No smoothing or interpolation was applied to the data. **b**, Constant-momentum cuts of the spin-flip cross-section through a pinch point at $\mathbf{q} = (2, 2, 0)$ and nodal point at $(2, 2, 1)$ integrated over $\ell \pm 0.2$. Solid lines are a fit to the sum of a Lorentzian function centred on the elastic line and a damped oscillator form $S(E) = \dfrac{(n+1)2\Gamma E}{\left(E^2 - E_q^2\right)^2 + (2\Gamma E)^2}$, where n is the thermal population factor, Γ a relaxation rate and E_q the characteristic energy scale. **c**, Constant-energy transfer cuts, integrated over $E \pm 0.25$ meV, showing the energy evolution of momentum-dependent scattering, which becomes doubly peaked above 5 meV. Error bars represent one standard deviation.
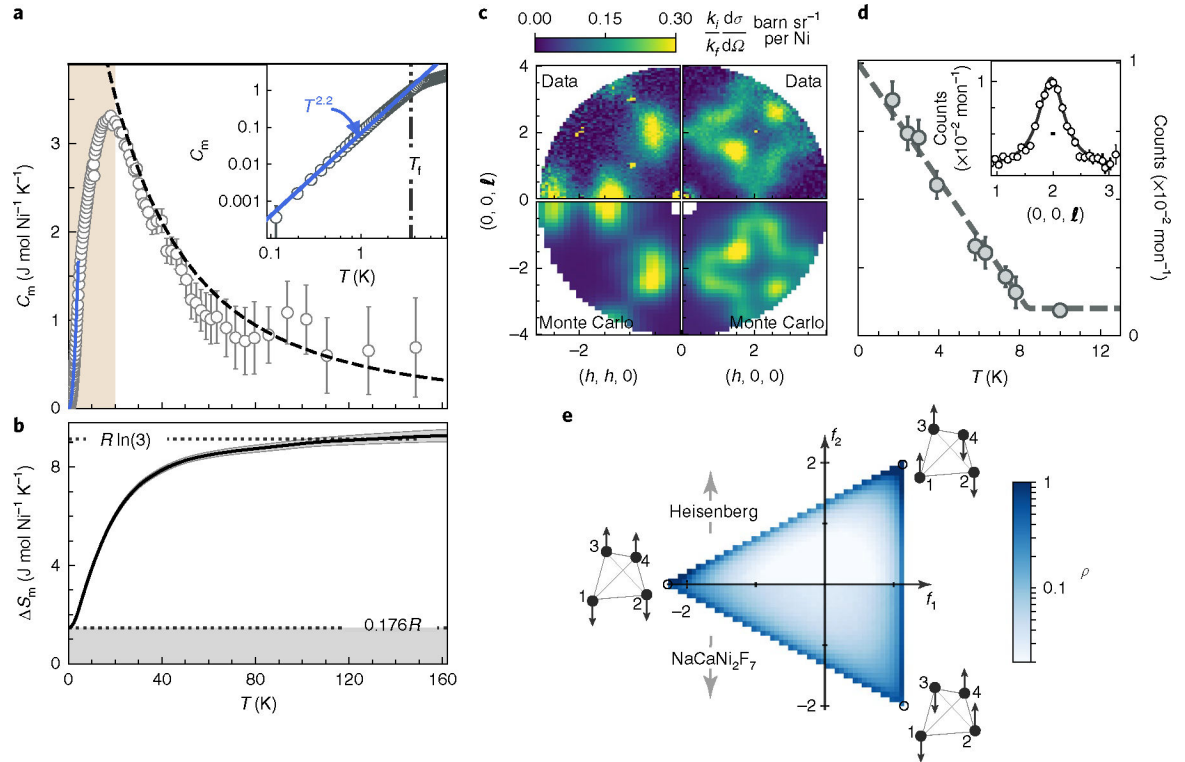
Fig. 4 |. Specific heat and elastic neutron scattering revealing spin freezing in NaCaNi$_2$F$_7$.
a, Magnetic specific heat. Dashed line is a classical Monte Carlo simulation and solid line is a fit to $C_m(T) = AT^\alpha$, with $A = 0.07(1)$ and $\alpha = 2.2(1)$. Light shading indicates the classical to quantum crossover regime. Inset shows the low-temperature region. **b**, Magnetic entropy obtained by integration of C/T between $T = 150$ K and 100 mK, corresponding to 84% of $R\ln(3)$. **c,** Diffuse elastic ($E = 0$) magnetic scattering, integrated over the resolution window of ±0.37 meV and obtained by subtracting $T = 40$ K data from that at 1.8 K. Lower quadrants display disorder and configuration-averaged ground state Monte Carlo structure factors. **d**, Temperature-dependent intensity of the diffuse elastic scattering around $\mathbf{q} = (0, 0, 2)$, dashed line is $(1 - T/T_f)^{2\beta}$, with $T_f = 8.2$ K and $\beta = 0.5$. Inset shows the $T = 1.8$ K line shape across the pinch point, integrated over $-0.1 < (h, h, 0) < 0.1$, the horizontal dash denotes the instrumental resolution. Error bars represent one standard deviation. **e**, Histogram of bond vector order parameter components (f_1, f_2) from classical Monte Carlo simulations for the Heisenberg and exchange models relevant to NaCaNi$_2$F$_7$ including exchange disorder. Extremal spin configurations corresponding to collinear spin arrangements are shown.